10/5-19-97 JSD

SANDIA REPORT

SAND97-8255 • UC-1425
Unlimited Release
Printed April 1997

M9705 3035

Optimum Conditions for Composites Fiber Coating by Chemical Vapor Infiltration

S. K. Griffiths, R. H. Nilson

Prepared by
Sandia National Laboratories
Albuquerque, New Mexico 87185 and Livermore, California 94550
for the United States Department of Energy
under Contract DE-ACO4-94AL85000

Approved for public release, distribution is unlimited.

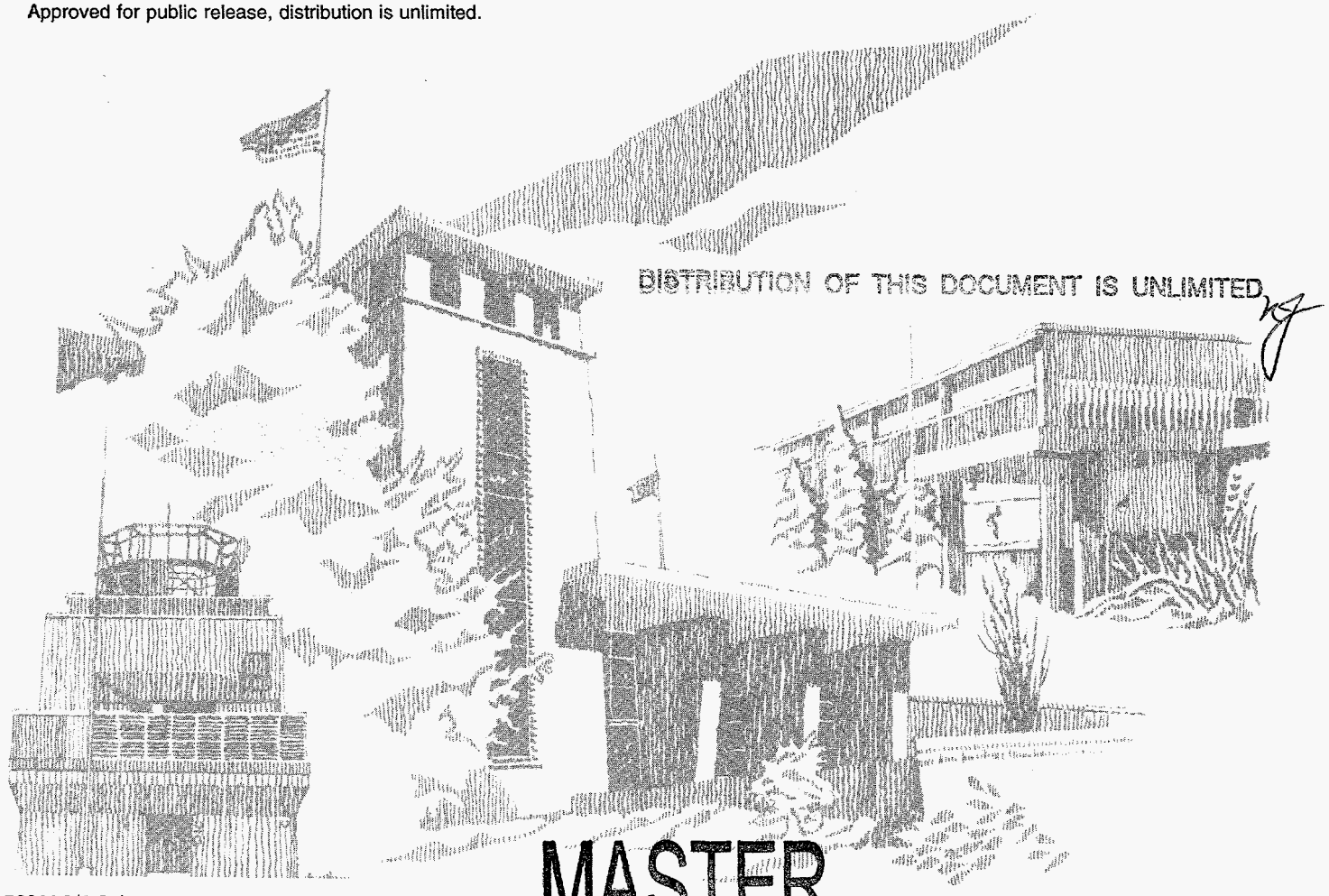

Issued by Sandia National Laboratories, operated for the United States Department of Energy by Sandia Corporation.

UC-1425

SAND97-8255
Unlimited Release
Printed April 1997

Optimum Conditions for Composites Fiber Coating by Chemical Vapor Infiltration

Stewart K. Griffiths and Robert H. Nilson
Sandia National Laboratories
Livermore, California 94551-0969

A combined analytical and numerical method is employed to optimize process conditions for composites fiber coating by chemical vapor infiltration (CVI). For a first-order deposition reaction, the optimum pressure yielding the maximum deposition rate at a preform center is obtained in closed form and is found to depend only on the activation energy of the deposition reaction, the characteristic pore size, and properties of the reactant and product gases. It does not depend on the preform specific surface area, effective diffusivity or preform thickness, nor on the gas-phase yield of the deposition reaction. Further, this optimum pressure is unaltered by the additional constraint of a prescribed deposition uniformity. Optimum temperatures are obtained using an analytical expression for the optimum value along with numerical solutions to the governing transport equations. These solutions account for both diffusive and advective transport, as well as both ordinary and Knudsen diffusion. Sample calculations are presented for coating preform fibers with boron nitride.

Introduction

Chemical vapor infiltration (CVI) is widely used in advanced composites manufacturing to deposit carbon, silicon carbide, boron nitride and other refractory materials within porous fiber preforms [1,2,3]. These deposition processes, employing a variety of chemistries, are usually performed in large batch furnaces at reduced pressures and elevated temperatures. In-furnace times typically range from a few hours to even weeks, resulting in costs ranging from $100 to over $1000 per kg for high-temperature high-performance composites [4]. Even under ideal conditions the processing time for these materials represents a significant fraction of the finished product cost, so optimizing processes conditions is important. In addition to the obvious benefit of lower product costs, lower prices are important to increasing the commercial applications for these materials, now largely limited to military uses.

The most common application of CVI in composites manufacturing is in densifying the preform. In this use, reactant gases are employed to deposit solids within a fiber preform with the intent of filling all or most of the inter-fiber void. These solids bind the fibers together and form the continuous matrix of the composite. A second common use of CVI is in coating the preform fibers prior to densification. These coatings serve as high-temperature oxidation inhibitors and as debonding agents to permit limited motion between the fibers and the composite matrix. Such motion is desirable as it improves the mechanical properties of a composite.

Most previous analyses of CVI have focused on the densification problem [5,6,7,8]. This is a difficult problem because the preform void fraction is altered significantly by the deposition process. The evolving microstructure strongly affects reactant transport through the preform, and so must be addressed in any meaningful analysis of densification. Because of this difficulty, most analyses of densification have employed numerical methods. Here we treat the simpler problem of fiber coating. In this case, the microstructure may be considered invariant through the deposition process, so long as the coating thickness remains a very small fraction of the original fiber size.

Many factors influence the optimum conditions for preform fiber coating. In some cases, high uniformity of the deposited coating may be required to obtain desired mechanical properties. In others, a specific temperature may be required to obtain a desired morphology of the deposited material. In still other cases, specific process conditions may be required either to induce or to inhibit certain gas-phase reactions, such as those involved in the production of necessary deposition precursors or those leading to undesirable gas-phase nucleation of particles. Here, however, we will address the issue of maximizing the deposition rate at the preform center. This condition is of practical interest because it minimizes the time required to deposit a coating of minimum acceptable thickness throughout a preform.

In this study we employ a combined analytical and numerical method to maximize the centerline deposition rate for CVI fiber coating processes involving a first-order deposition reaction. Two general expressions for the optimum pressure and optimum temperature are first derived using analytical methods. The optimum pressure is then obtained in closed form, while the optimum temperature is determined with the aid of numerical solutions to the governing diffusion and reaction equations. These numerical solutions account for advective transport of the reactant gases, as well as both ordinary and Knudsen diffusion. Finally, we consider the influence on the optimum pressure of a constraint on the deposition uniformity. In this case, the optimum pressure maximizing centerline deposition rates is obtained in closed form using the method of Lagrange multipliers.

The results of this analysis are presented in a dimensionless form readily applicable to a range of preform thicknesses, fiber diameters, fiber volume fractions, and deposition chemistries. To illustrate the application of these results to a practical problem, the optimum process conditions are determined for a sample problem in which a boron nitride coating is deposited from boron trichloride and ammonia.

Governing Equations

To calculate centerline deposition rates, we consider the region within a preform, as shown in Fig. 1. Diffusive and advective transport in the volume between fibers and the accompanying reactant depletion due to deposition on fiber surfaces are described by continuity equations for each gas-phase species, along with momentum and energy equations for the gas mixture. Here we consider one-dimensional transport in which species concentrations vary only with the transverse position through the preform thickness. Under this idealization, conservation of mass for a single reactive species may be written as

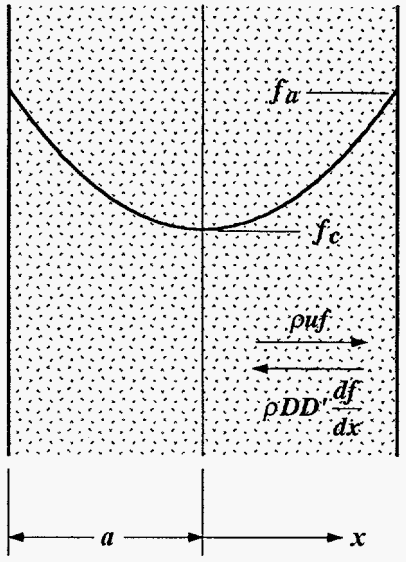

Figure 1. Schematic cross-section of a porous fiber preform. Reactants diffuse from the preform surfaces toward the center, and are depleted by deposition on fiber surfaces.

$$\frac{d}{dx}\left(\rho DD'\frac{df}{dx}\right) - \frac{d}{dx}(\rho uf) = Ss_v \qquad (1)$$

where x is the distance from the preform center, ρ is the gas molar density, f is the reactive species mole fraction, D is the effective coefficient of binary diffusion for the reactive species, D' is the dimensionless effective diffusivity of the porous preform, and u is the local molar-average fluid speed. The preform specific surface area, s_v, is the fiber surface area per unit volume, and S is the surface deposition rate.

Again assuming one-dimensional transport, continuity for the combined reactive and inert species can be expressed as

$$\frac{d}{dx}(\rho u) = \psi Ss_v \qquad (2)$$

where the parameter ψ is the net molar yield of gaseous products per mole of reactant; that is, the molar ratio of gaseous products less reactants to reactants. By this definition, values of the parameter are

limited to $\psi \geq -1$ since we are considering here only one reactive species. The limiting value of $\psi = -1$ corresponds to a simple single-species deposition reaction yielding solids but no gas-phase products.

If the deposition process is a first-order reaction having an Arrhenius temperature dependence, the surface reaction rate, S, can be expressed as the product of the surface impingement rate and a reaction probability, ϕ. In terms of the gas molar density and reactant mole fraction this is

$$S = \frac{\overline{v}}{4}\rho f \phi \quad \text{where} \quad \phi = b e^{-E_a/RT} \tag{3}$$

The mean molecular speed, $\overline{v}$, of the reactive species is given by

$$\overline{v} = \left(\frac{8RT}{\pi m}\right)^{1/2} \tag{4}$$

where R is the ideal gas constant, T is the gas temperature, and m is the reactive species molecular weight. The parameters b and E_a are the surface reaction pre-exponential constant and the apparent activation energy, respectively.

The coefficient of diffusion in Eq. (1) must account for both ordinary and Knudsen diffusion. At high gas densities, collisions of the reactive species with gas molecules are much more common than are collisions with fiber surfaces. In this limit, the diffusive flux of the reactive species is governed by ordinary diffusion. At sufficiently low pressures or sufficiently high temperatures, however, the mean free path of the reactive species becomes large relative to the size of the inter-fiber pores. In this limit, collisions of the reactive species with fiber surfaces are predominant, and the diffusive flux is controlled by Knudsen diffusion. To account for both of these conditions, the overall effective coefficient of binary diffusion for the reactive species can be approximated by the Bonsanquet interpolation formula [9],

$$\frac{1}{D} = \frac{1}{D_m} + \frac{1}{D_{\text{Kn}}} \tag{5}$$

where D_m denotes the effective binary coefficient of ordinary diffusion for the reactive species in the gas mixture, and D_{Kn} denotes the coefficient of Knudsen diffusion for the reactive species in the inter-fiber volume. Based on simple kinetic theory, Eq. (5) may be rewritten as [10]

$$D = \frac{\overline{v}\lambda}{3}\frac{\alpha d}{d + \alpha\lambda} = \frac{\overline{v}d}{3}\frac{\alpha \text{Kn}}{1 + \alpha \text{Kn}} \tag{6}$$

where $\overline{v}$ is again the mean molecular speed of the reactive species, and $\text{Kn} = \lambda/d$ is the Knudsen number based on properties of the reactive species and the inter-fiber pore size. The effective mean free path for the reactive species alone is given by

$$\lambda = \frac{RT}{\sqrt{2}\pi N \sigma^2 p} \tag{7}$$

where p is the total pressure, N is the Avogadro number, and σ is the molecular diameter of the reactive species.

The parameter α in Eq. (6) is the ratio of the effective binary coefficient of ordinary diffusion for the reactive species and the mixture of other void gases to the coefficient of ordinary self diffusion for the reactive species. As shown in the Appendix, this parameter depends only on the composition of the gas mixture and is independent of both the pressure and temperature for ideal gases. Thus for fixed gas composition, the parameter α is constant.

The continuity equations (1) and (2) must be accompanied by momentum and energy equations. In this analysis, we supplant the energy equations with an assumption that all gas species are at a uniform and constant temperature, T. Likewise, the momentum equation is replaced with an assumption that the pressure is uniform over the preform thickness.

The governing transport equations are closed using an ideal gas equation of state, $p = \rho RT$. Because both the pressure and temperature are uniform and constant, this relation requires that the gas molar density within the preform is also uniform and constant.

To complete the mathematical statement of the transport and deposition problem, boundary conditions must be specified for the reactive species fraction and fluid speed. The second-order equation governing the reactive species requires two conditions. One is imposed by symmetry, requiring that the gradient of the reactive species vanish at the origin. For the second we assume that the reactive species mole fraction is fixed at the preform surface.

$$\frac{df}{dx} = 0 \ \text{ at } \ x = 0 \qquad f = f_a \ \text{ at } \ x = a \tag{8a,b}$$

In addition, the first-order equation governing the fluid speed requires a single boundary condition. Again this is obtained from a symmetry condition at the preform center,

$$u = 0 \ \text{ at } \ x = 0 \tag{9}$$

requiring no flow into or out of the plane of symmetry.

To normalize the governing equations, we introduce a dimensionless position, $z = x/a$, and two dimensionless dependent variables, $f^* = f/f_a$ and $u^* = ua/DD'$. Note that the normalized velocity u^* is equivalent to a local Peclet number, indicating the relative magnitudes of the advective and diffusive fluxes of the reactive species. Applying these definitions to the transport equations yields the dimensionless governing equations

$$\frac{d}{dz}\left(\frac{df^*}{dz}\right) - \frac{d}{dz}(u^*f^*) + \frac{1}{D}\frac{\partial D}{\partial f^*}\left(\frac{df^*}{dz} - u^*f^*\right)\frac{df^*}{dz} = \beta f^* \qquad (10)$$

for the reactive species, and

$$\frac{du^*}{dz} + \frac{u^*}{D}\frac{\partial D}{\partial f^*}\frac{df^*}{dz} = \psi^*\beta f^* \qquad (11)$$

for total species conservation. The constant β on the right of these equations is

$$\beta = \frac{Ss_v a^2}{\rho DD' f} = \frac{3}{4}\frac{1+\alpha\mathrm{Kn}}{\alpha\mathrm{Kn}}\,\xi^2\, e^{-E_a/RT} \qquad (12)$$

and the new parameters appearing here are the normalized preform thickness,

$$\xi^2 = \frac{b\, s_v a^2}{dD'} \qquad (13)$$

and the normalized reaction yield, $\psi^* = \psi f_a$. Boundary conditions for the normalized variables follow from Eqs. (8) and (9) in the obvious manner.

The usual interpretation of the parameter β, referred to here as the deposition modulus, is that it is the square of the ratio of the characteristic time for diffusion to the characteristic time for surface deposition. In this view it is equivalent to the square of the Thiele modulus commonly appearing in analyses of porous-bed catalysis. Another useful interpretation of this parameter is that it is the ratio of two rates – the rate of deposition on the preform fiber surfaces, $Ss_v a$, to the maximum rate of diffusive transport, $\rho DD' f_a/a$. Thus when β is small, the actual rate of diffusive transport will be less than this maximum, and the mean gradient of the reactant fraction will be smaller than the maximum value of f_a/a. Under any of these interpretations, small values of β are associated with high uniformity of both the reactant fraction and coating thickness.

One additional relation can be obtained from Eqs. (1) and (2) by integrating each equation once and combining the two results. This yields

$$u^* = \frac{\psi^*}{1+\psi^* f^*}\frac{df^*}{dz} \qquad (14)$$

giving the normalized fluid speed in terms of the normalized reactant mole fraction and its derivative alone. This relation applies everywhere and so is useful in separating the coupled reactive species and total conservation equations. Substituting Eq. (14) into either Eq. (10) or (11) to eliminate u^* gives

$$\frac{d}{dz}\left(\frac{1}{1+\psi^* f^*}\frac{df^*}{dz}\right) + \frac{1}{1+\psi^* f^*}\left(\frac{df^*}{dz}\right)^2\frac{1}{D}\frac{\partial D}{\partial f^*} = \beta f^* \qquad (15)$$

This species equation can now be solved without explicit knowledge of the local fluid speed. Fluid speeds can be computed after the fact from Eq. (14).

Equation (15) further provides useful insight into the relation between advective and diffusive fluxes of the reactive species. In dimensional form the advective flux at any position is ρuf, while the magnitude of the diffusive flux is $\rho DD'\, df/dx$. The local ratio of advective to diffusive fluxes is therefore given by

$$\frac{\rho uf}{\rho DD'\, df/dx} = \frac{u^* f^*}{df^*/dz} = \frac{\psi^* f^*}{1+\psi^* f^*} \approx \frac{\psi^*}{1+\psi^*} \qquad (16)$$

where the approximate equality on the right is due to the fact that $f^* \approx 1$ when the deposition rate is fairly uniform over the preform thickness. Taking into account the signs for each flux, we see that the total flux of the reactive species differs from the diffusive flux by a factor of $1/(1+\psi^* f^*)$. This is also apparent in Eq. (15), where this term serves as an apparent diffusivity in what otherwise appears as a simple diffusion-reaction equation. When ψ^* is positive, the total flux of the reactive species is therefore reduced by the flow of gas toward the preform surface. When ψ^* is negative, the total flux is increased by flow toward the preform center. Note that the total flux is quite sensitive to the deposition chemistry. For a net production of only one mole of gas per mole of reactant, $\psi = 1$, the advective transport reduces the net flux of reactive species toward the preform center by up to a factor of two. As such, this advective inhibition of diffusion in the inter-fiber volume may significantly reduce deposition uniformity when the reactant fraction is large.

The derivative of the diffusivity on the right of Eq. (15) is the order of the diffusivity with respect to the reactant fraction. From Eq. (6) it is given by

$$\frac{1}{D}\frac{\partial D}{\partial f^*} = \frac{1}{1+\alpha \mathrm{Kn}}\,\frac{1}{\alpha}\frac{\partial \alpha}{\partial f^*} \tag{17}$$

However, under a rather broad range of conditions its value is near zero. For a simple binary mixture of the reactant and a single diluent gas, $\partial\alpha/\partial f^*$ is exactly zero because binary diffusivities of low-pressure gases do not depend on species concentrations. Further, the effective binary diffusivity of the reactant and a gas mixture also shows no dependence on the reactant fraction provided that the composition of the mixture does not vary with the reactant fraction. This of course is the case whenever the reactant fraction is small.

Under the simplifying assumption that the diffusivity is independent of the reactant fraction, the governing conservation Eq. (15) may be written as

$$\frac{d}{dz}\left(\frac{1}{1+\psi^* f^*}\frac{df^*}{dz}\right) = \beta f^* \tag{18}$$

In the limit $\psi^* \to 0$, Eq. (18) possesses the well known solution [11]

$$f^* = \frac{\cosh(\sqrt{\beta}\, z)}{\cosh(\sqrt{\beta}\,)} \tag{19}$$

No such closed-form solution exists for the more general case $\psi^* \neq 0$. The general form of Eq. (18) can be solved [12] for small values of the deposition modulus, β, though as we will see later, such solutions are not applicable to the problem of interest. Fortunately, very accurate numerical solutions to the boundary value problem posed by Eqs. (8) and (18) are readily obtained using a numerical shooting technique.

Normalization of Variables

To solve generally for the optimum conditions and to plot resulting deposition rates, it is useful to rewrite the pressure, temperature, density and deposition rate in terms of normalized variables. For this purpose, the normalized values are defined as $p^* = p/p_{\mathrm{R}}$, $T^* = T/T_{\mathrm{R}}$, and $\rho^* = \rho/\rho_{\mathrm{R}}$. Similarly, the normalized deposition rate and molecular speed are $S^* = S/S_{\mathrm{R}}$ and $\bar{v}^* = \bar{v}/\bar{v}_{\mathrm{R}}$. The reference temperature, density and speed for a first-order deposition reaction are taken as

$$T_{\mathrm{R}} = \frac{E_a}{R} \quad \rho_{\mathrm{R}} = \frac{\alpha}{\sqrt{2}\,\pi d N \sigma^2} \quad \bar{v}_{\mathrm{R}} = \left(\frac{8RT_{\mathrm{R}}}{\pi m}\right)^{1/2} \tag{20}$$

We additionally require that the reference density, pressure and temperature satisfy the ideal gas equation of state, $p_{\mathrm{R}} = \rho_{\mathrm{R}} R T_{\mathrm{R}}$.

The normalized density and normalized molecular speed follow directly from the reference values.

$$\rho^* = \frac{p^*}{T^*} = \frac{1}{\alpha \mathrm{Kn}} \quad \text{and} \quad \bar{v}^* = \sqrt{T^*} \tag{21a,b}$$

Now taking $S_{\mathrm{R}} = b\,\rho_{\mathrm{R}}\bar{v}_{\mathrm{R}} f_a/4$ as the reference deposition rate, the normalized deposition rate may be written as

$$S^* = \rho^*\,\bar{v}^* f^* e^{-1/T^*} = \frac{p^*}{\sqrt{T^*}} f^* e^{-1/T^*} \tag{22a,b}$$

A second useful normalization of the deposition rate is the simple modification of S^* given by $S^{**} = \xi^2 S^*$. Note that the normalized centerline deposition rate can be obtained from Eqs. (22a,b) simply by taking $f^* = f_c^*$, where f_c^* is the normalized reactant fraction at $z = 0$. The pressure, temperature and all other variables in these expressions are uniform over the preform thickness.

Finally, Eq. (12) may be rewritten to obtain an expression for the deposition modulus that depends only on the normalized pressure, temperature and preform thickness.

$$\beta = \frac{3}{4}\,\frac{p^* + T^*}{T^*}\,\xi^2\, e^{-1/T^*} \tag{23}$$

Thus, since β and ψ^* are the only parameters in Eqs. (10) and (11), the normalized deposition rate at the preform center is uniquely determined by the normalized pressure, temperature, preform thickness and reaction yield.

Discussion of Deposition Rates

The deposition modulus at low temperatures is small, and the profile of the reactant concentration through the preform thickness is very uniform. In this case, the deposition rate at the center is nearly as large as that at the preform surface. With increasing temperature, the deposition modulus increases and the reactant concentration at the preform center falls. In this case, the centerline deposition rate becomes small relative to that at the surface. This behavior is illustrated in Fig. 2. Here we see that the normalized centerline reactant fraction falls monotonically with increasing values of the deposition modulus. The centerline reactant fraction does not exhibit any sort of

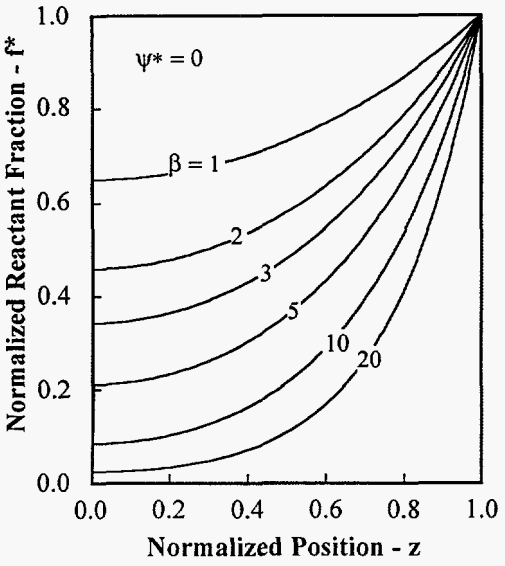

Figure 2. Distribution of normalized reactant fraction through the preform thickness. Reactant fractions depend only on the dimensionless reaction yield, ψ^* and the deposition modulus, β.

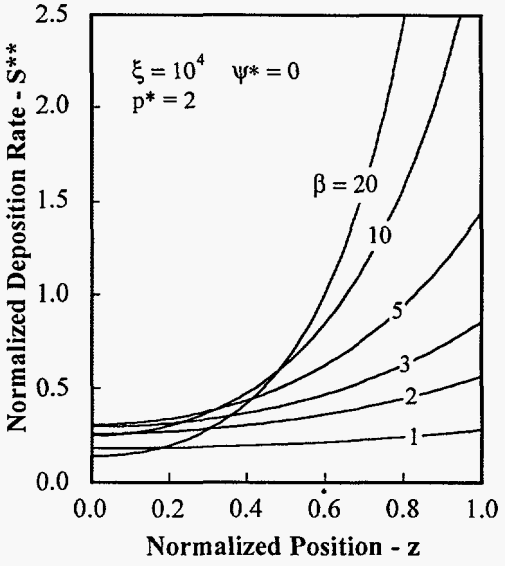

Figure 3. Normalized deposition rate through preform thickness. Maximum centerline deposition rate occurs at a specific value of the deposition modulus, β; its value is $\beta \approx 4.453$ for the conditions shown.

maximum, as is well known, and the deposition uniformity, $U = f_c^*$, falls smoothly as the deposition modulus is increased.

Although uniformity always falls with increasing values of the deposition modulus, this observation provides no insight into how the magnitude of the centerline deposition rate varies as the temperature and deposition modulus are increased. Low temperatures necessarily correspond to small deposition rates. As such, the deposition rate on the centerline is comparable to that at the surface when the temperature is low and the deposition modulus is small, but the rates everywhere within the preform, including the preform center, are small. In contrast, when the temperature is high and the deposition modulus is large, the deposition rate at the preform surface is large, but reactant depletion through the preform thickness is severe. In this case, the deposition rate at the preform center is very small compared to that at the surface, and the centerline deposition rate is again small. Between these extremes of temperature lies the maximum centerline deposition rate.

Fig. 3 shows sample calculations of the normalized deposition rate through the preform thickness. We see that the deposition rate at the preform surface increases monotonically with increasing values of the deposition modulus. At the preform center, however, the deposition rate increases only up to a value of $\beta \approx 4$. At still larger values the centerline rate begins to fall, gradually approaching zero as $\beta \to \infty$. Thus for the conditions shown, the centerline deposition rate exhibits a maximum when the deposition modulus is about $\beta \approx 4$.

The conditions giving rise to the maximum centerline deposition rate do not yield the maximum surface rate, nor do they yield the maximum mean deposition rate. This is shown in Fig. 4, where the centerline, surface and mean normalized deposition rates are shown as a function of the normalized temperature. Here we see that both the surface and mean rates increase smoothly with increasing temperature and that only the centerline rate exhibits a maximum. For the conditions shown, this maximum occurs at $T^* \approx 0.0491$, corresponding to $\beta \approx 4.453$ and a deposition uniformity of $U = f_c^* \approx 0.239$.

Maximum Centerline Deposition Rate

To identify optimum conditions for the CVI fiber coating process, we seek to maximize the deposition rate at the preform center. This maximum deposition rate is defined by the requirement that the variation

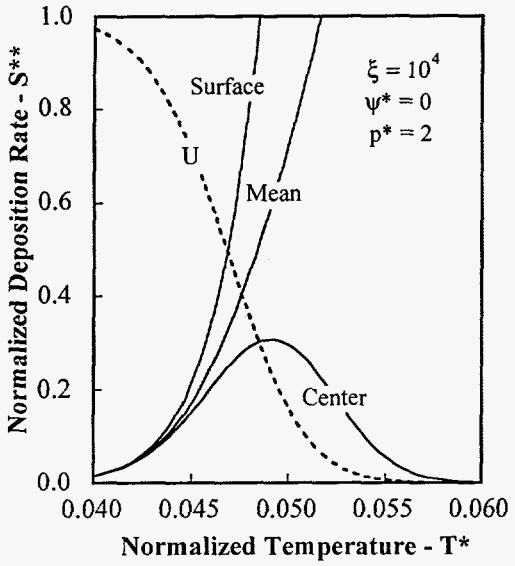

Figure 4. Surface, mean and centerline deposition rates. For a given pressure, the maximum centerline deposition rate occurs at a specific temperature and corresponding value of the deposition modulus.

in rate with respect to both the pressure and temperature is zero. Because the pressure, temperature and deposition rate are all normalized only by constants, these conditions apply equally to the dimensional and normalized derivatives. The conditions for the maximum in terms of the normalized variables are

$$\frac{\partial S^*}{\partial p^*} = 0 \quad \text{and} \quad \frac{\partial S^*}{\partial T^*} = 0 \qquad (24a,b)$$

where both derivatives of the deposition rate are evaluated at $z = 0$. Now using Eq. (22b) for the normalized deposition rate, Eq. (24a) may be written as

$$\frac{1}{S^*}\frac{\partial S^*}{\partial p^*} = \frac{1}{p^*} + \frac{\beta}{f_c^*}\frac{\partial f_c^*}{\partial \beta}\frac{1}{\beta}\frac{\partial \beta}{\partial p^*} = 0 \qquad (25)$$

where again f_c^* is the normalized reactant fraction at the preform center. Similarly, Eq. (24b) may be written as

$$\frac{1}{S^*}\frac{\partial S^*}{\partial T^*} = \frac{1}{T^*}\left(\frac{1}{T^*} - \frac{1}{2}\right) + \frac{\beta}{f_c^*}\frac{\partial f_c^*}{\partial \beta}\frac{1}{\beta}\frac{\partial \beta}{\partial T^*} = 0 \qquad (26)$$

The derivatives of the deposition modulus with respect to pressure and temperature can now be obtained from Eq. (23). They are

$$\frac{1}{\beta}\frac{\partial \beta}{\partial p^*} = \frac{1}{p^* + T^*} \qquad (27)$$

and

$$\frac{1}{\beta}\frac{\partial \beta}{\partial T^*} = \left(\frac{1}{T^*} - \frac{p^*}{p^* + T^*}\right)\frac{1}{T^*} \qquad (28)$$

Combining these results with Eqs. (25) and (26) then yields

$$1 + \frac{T^*}{p^*} = -\frac{\beta}{f_c^*}\frac{\partial f_c^*}{\partial \beta} \qquad (29)$$

for Eq. (24a), and

$$\frac{1}{T^*} - \frac{1}{2} = -\frac{\beta}{f_c^*}\frac{\partial f_c^*}{\partial \beta}\left(\frac{1}{T^*} - \frac{p^*}{p^* + T^*}\right) \qquad (30)$$

for Eq. (24b). This pair of equations, along with a solution to the boundary value problem to obtain the derivative $\partial f_c^*/\partial \beta$, can now be solved to obtain the optimum pressure and optimum temperature yielding the maximum centerline deposition rate.

We would generally expect that Eqs. (29) and (30) must be solved together to obtain the optimum pressure and temperature as a pair. Surprisingly, this is not the case here. Combining these to eliminate the derivative on the right of each yields

$$\frac{1}{T^*} - \frac{1}{2} = \left(1 + \frac{T^*}{p^*}\right)\left(\frac{1}{T^*} - \frac{p^*}{p^* + T^*}\right) \qquad (31)$$

which can be rearranged to eliminate the normalized temperature and give the simple result

$$p^* = 2 \qquad (32)$$

for the optimum pressure alone. Using the definition of the normalized pressure, the dimensional optimum pressure is

$$p = 2p_R = \frac{\sqrt{2}\,\alpha E_a}{\pi d N \sigma^2} \qquad (33)$$

This is a remarkable result in that the optimum pressure does not depend on the process temperature, the preform specific surface area, or the preform thickness. It depends only on the activation energy for the deposition reaction, the composition of the gas mixture, species properties of the mixture gases, and the inter-fiber pore size.

Using this result for the optimum pressure, the optimum temperature can now be obtained from Eq. (29) as

$$1 + \frac{T^*}{2} = -\frac{\beta}{f_c^*}\frac{\partial f_c^*}{\partial \beta} \tag{34}$$

Given $\partial f_c^*/\partial\beta$ as a function of T^* from numerical solutions to Eq. (18), this expression can be solved for the optimum normalized temperature.

For the special case of $\psi^* \to 0$, again corresponding to no net reaction yield or to a very small reactant fraction, Eq. (19) yields

$$\frac{\beta}{f_c^*}\frac{\partial f_c^*}{\partial \beta} = -\frac{1}{2}\sqrt{\beta}\tanh\sqrt{\beta} \tag{35}$$

giving an optimum temperature specified by

$$2 + T^* = \sqrt{\beta}\tanh\sqrt{\beta} \tag{36}$$

Under the further restriction that $\xi \to \infty$, corresponding to $T^* \to 0$, the last term on the left of Eq. (36) may be neglected. This special case yields $\beta \approx 4.2656$ and a corresponding centerline reactant fraction of $f_c^* \approx 0.2495$. The optimum temperature can then be obtained by using the optimum pressure, $p^* = 2$, in Eq. (23). This gives

$$\left(\frac{2}{T^*} + 1\right) e^{-1/T^*} = \frac{4}{3}\frac{\beta}{\xi^2} \approx \frac{5.6875}{\xi^2} \tag{37a,b}$$

This equation can be solved easily by successive substitution. Using a guessed value of the temperature in the first factor on the left of Eq. (37a), the exponential term is inverted to obtain an improved value for the guess. When repeated, this procedure converges in just a few cycles for all conditions of practical importance. For $\xi = 10^4$, the temperature obtained from Eq. (37b) is $T^* = 0.04898$. The maximum centerline deposition rate can be computed from Eqs. (19) and (22b) once the pressure and temperature have been obtained.

When T^* is not small, Eqs. (36) and (37a) must be solved together as an implicitly coupled system. Similarly, when ψ^* is not negligible, Eqs. (34) and (37a) must be solved together, along with an appropriate solution of Eq. (18) to provide $\partial f_c^*/\partial\beta$ and f_c^*.

Optimum Conditions

Sample calculations of the optimum pressure and optimum temperature and the maximum centerline deposition rate are shown in Fig. 5 as a function of the normalized preform thickness, ξ. These results are all for the special case of negligible reaction yield, $\psi^* = 0$. As noted above, the optimum pressure is independent of ξ and is given by $p^* = 2$. The most surprising feature of this figure is that the deposition modulus and deposition uniformity at the optimum conditions vary by only about 15% as the normalized preform thickness varies by eight orders of magnitude. In essence, the optimum conditions yielding maximum centerline deposition rate occur when the centerline reactant fraction is $f_c^* = U \approx 0.25$, regardless of the preform thickness. This result provides a very simple practical method of determining the optimum conditions. In addition, because the optimum deposition modulus is nearly constant at $\beta \approx 4.3$, Eq. (12) provides a simple means of adjusting the process temperature to maintain the optimum value as the preform thickness is varied.

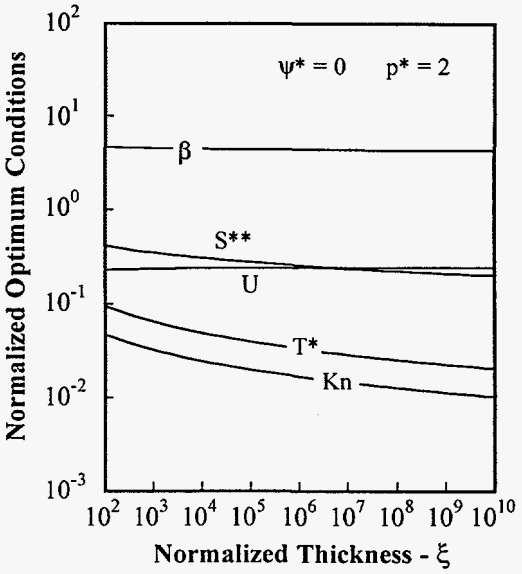

Figure 5. Normalized optimum conditions as a function of normalized preform thickness. Optimum deposition uniformity is insensitive to preform thickness, but maximum deposition rates fall as $S \propto S^{**}/\xi^2$.

Despite these weak variations in the optimum process conditions, the maximum normalized deposition rate varies inversely with the square of the preform thickness. The reason for this is that the normalized temperature is small over the range of conditions shown. In this limit of $T^* \to 0$, Eqs. (22b) and (23) can be combined to express the normalized deposition rate in terms of the normalized preform

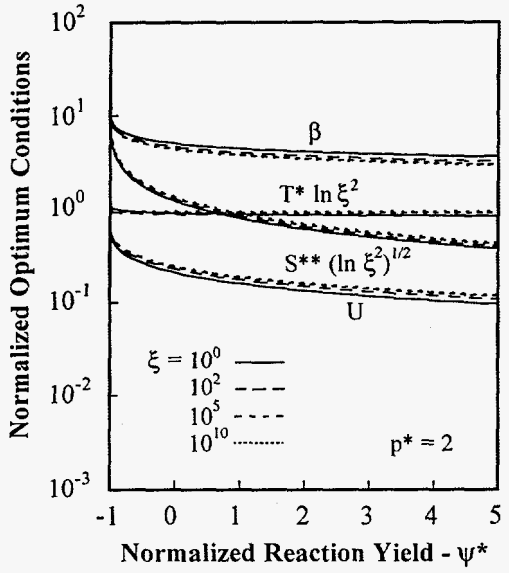

Figure 6. Normalized optimum conditions as a function of normalized reaction yield. Larger reaction yields require slightly lower temperatures and give significantly reduced maximum deposition rates.

thickness: $S^* \approx 4\sqrt{T^*}\beta f_c^*/3\xi^2$. Thus the maximum deposition rate differs by less than a factor of three from a squared dependence on the preform thickness as the thickness varies from 10^2 to 10^{10}.

The results presented so far have been for the special case of no normalized reaction yield, $\psi^* = 0$. In general this parameter will not be small unless the ambient reactant fraction is negligible, $f_a << 1$. To examine the effects of non-zero reactant yields, we have computed the optimum temperature, deposition modulus, deposition rate, and centerline reactant fraction for a wide range of ψ^*. Note that the optimum pressure does not depend on ψ^*, and so is still given by $p^* = 2$. These results are shown in Fig. 6. By the noted additional normalization of the temperature and deposition rate, this single figure gives the optimum conditions for all practical values of both the normalized reaction yield and normalized preform thickness.

We see in Fig. 6 that the optimum deposition modulus, uniformity at the optimum, and the maximum deposition rate all decrease significantly with increasing values of the normalized reactant yield. The reason for this is that positive values of the reaction yield correspond to a net production of gas in the deposition reaction and a corresponding flow away from the center toward the preform surface. This outward flow impedes the inward diffusion of the reactive species, and so gives rise to greater nonuniformity, lower reactant fractions at the preform center, and correspondingly lower centerline deposition rates. This increased resistance to diffusion therefore requires a reduced temperature to maximize the centerline deposition rate. Note that although the normalized temperature appears nearly constant over this range of ψ^*, the very small variation present gives rise to a large effect on the optimum deposition modulus and the maximum centerline deposition rate. For this reason, the value of T^* is most accurately determined by solving Eq. (37a) using the value of β read from Fig. 6.

Character of Maximum Deposition Rate

Although Eqs. (32) and (34) define optimum conditions giving the maximum deposition rate at the preform center, they provide no insight into the character of this maximum. To gain this insight, we need to examine the variation of the deposition rate in the vicinity of the optimum conditions. This is depicted in Fig. 7. Here the normalized deposition rate is shown as a function of the normalized pressure, for fixed values of the normalized preform thickness. At each pressure along each curve, the corresponding temperature and normalized deposition rate are computed from Eqs. (30) and (22b). Using this approach, the centerline deposition rate is maximized with respect to the temperature, even though the pressure is not necessarily optimum.

We see in Fig. 7 that the deposition rate exhibits a weak one-sided maximum; at all pressures above the optimum value, the deposition rate is nearly constant. The reason for this lies in the tradeoff between the linear pressure dependence of the deposition and the nonlinear pressure dependence of the diffusivity. Combining Eqs. (25) and (26), and setting $\partial S^*/\partial T^* = 0$, Eq. (25) may be rewritten as

$$\frac{p^*}{S^*}\frac{\partial S^*}{\partial p^*} = \frac{T^*(2-p^*)}{2p^*(1-T^*)+2T^*} \qquad (38)$$

At very low pressures Knudsen diffusion is dominant, corresponding to $\alpha\mathrm{Kn} = \alpha\lambda/d = T^*/p^* >> 1$. In this limit, Eq. (38) yields a linear relation between the pressure and deposition rate.

$$\frac{p^*}{S^*}\frac{\partial S^*}{\partial p^*} \to 1 \quad \text{as} \quad p^* \to 0 \qquad (39)$$

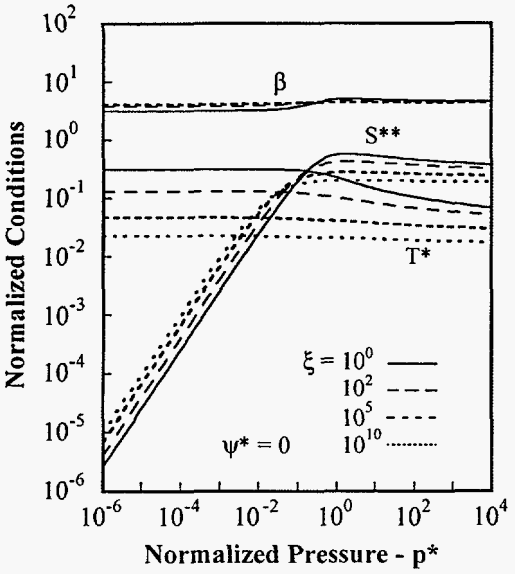

Figure 7. Normalized deposition rates near the optimum pressure. Deposition rates exhibit a weak one-sided maximum with the deposition rate falling slowly at pressures above the optimum.

Similarly, at high pressures ordinary diffusion is dominant, corresponding to $T^*/p^* << 1$. In this limit, the deposition rate gradually falls to a constant

$$\frac{p^*}{S^*}\frac{\partial S^*}{\partial p^*} \rightarrow -\frac{T^*}{2(1-T^*)} \quad \text{as} \quad p^* \rightarrow \infty \tag{40}$$

as the pressure increases without bound.

Optimum Pressure At Fixed Uniformity

The conditions yielding the unconstrained maximum centerline deposition rate give a deposition uniformity of only about 25%. While this may well be acceptable for some fiber coating processes, there are likely applications for which it is not. We now consider the problem of maximizing the centerline deposition rate, subject to an additional constraint that the deposition uniformity satisfies some minimum requirement. Assuming that the required uniformity is better than that obtained in the unconstrained case, the constrained maximum centerline deposition rate should occur when the uniformity constraint is just marginally satisfied. This permits replacing the inequality constraint of a minimum uniformity by an equality constraint that is satisfied exactly.

The constrained maximum deposition rate is defined by the requirement that the variation in rate with respect to all independent variables is zero along the direction of constant uniformity. To obtain this maximum we employ the method of Lagrange multipliers [13]. This technique introduces one new unknown constant for each constraint and yields one additional equation for each independent variable. The two new equations are

$$\frac{\partial S^*}{\partial p^*} - \kappa\frac{\partial U}{\partial p^*} = 0 \quad \text{and} \quad \frac{\partial S^*}{\partial T^*} - \kappa\frac{\partial U}{\partial T^*} = 0 \tag{41a,b}$$

where κ, the Lagrange multiplier, is the new unknown constant. Together with the original constraint on the deposition uniformity, this pair of equations can be solved for the optimum pressure and temperature yielding the constrained maximum centerline deposition rate.

Rearranging Eqs. (41a) and (41b) to eliminate κ yields

$$\frac{\partial S^*}{\partial p^*}\frac{\partial U}{\partial T^*} = \frac{\partial S^*}{\partial T^*}\frac{\partial U}{\partial p^*} \tag{42}$$

By the definition $U = S^*_c/S^* = f^*_c$, the derivatives of the uniformity with respect to pressure and temperature may be written as

$$\frac{1}{U}\frac{\partial U}{\partial p^*} = \frac{\beta}{f^*_c}\frac{\partial f^*_c}{\partial \beta}\frac{1}{\beta}\frac{\partial \beta}{\partial p^*} \tag{43}$$

and

$$\frac{1}{U}\frac{\partial U}{\partial T^*} = \frac{\beta}{f^*_c}\frac{\partial f^*_c}{\partial \beta}\frac{1}{\beta}\frac{\partial \beta}{\partial T^*} \tag{44}$$

Now using these results along with the definitions given previously in the left of Eqs. (25) and (26), Eq. (42) above can be expressed as

$$\frac{1}{\beta}\frac{\partial \beta}{\partial T^*} = \frac{p^*}{T^*}\left(\frac{1}{T^*} - \frac{1}{2}\right)\frac{1}{\beta}\frac{\partial \beta}{\partial p^*} \tag{45}$$

Finally, using the definitions of Eqs. (27) and (28) for the derivatives of the deposition modulus, Eq. (44) becomes

$$\frac{1}{T^*} - \frac{1}{2} = \left(1 + \frac{T^*}{p^*}\right)\left(\frac{1}{T^*} - \frac{p^*}{p^* + T^*}\right) \tag{46}$$

This is exactly the same as Eq. (31) obtained previously, and again this can be rearranged to give

$$p^* = 2 \quad \text{or} \quad p = \frac{\sqrt{2}\,\alpha E_a}{\pi d N \sigma^2} \tag{47}$$

Thus, we find that the optimum pressure maximizing the centerline deposition rate for a specified uniformity is the same as that obtained in the unconstrained problem. The optimum temperature in this case can now be obtained directly from the prescribed deposition uniformity and a numerical solution to Eq. (18).

This remarkable result suggests a strategy for optimizing process conditions in coating processes: first, the pressure is fixed at the optimum value; the temperature is then varied until the desired uniformity is obtained, keeping in mind that the maximum possible centerline deposition rate will occur at a uniformity of about 25%. Using this strategy, the time-consuming process of empirically varying both the pressure and temperature to produce at once both the desired uniformity and maximum deposition rate can be avoided.

This result also suggests a possible strategy for minimizing in-furnace times for the more complex densification process. As described earlier, preform transport properties vary significantly during densification, and this might have a strong influence on the optimum time-dependent pressure and temperature histories. This influence appears, however, to be limited to effects on the temperature. The optimum pressure does not depend on transport properties, but instead depends only on the preform effective pore diameter, and pore diameters fall by at most about an order of magnitude during most densification processes. We also know from Fig. 7 that deposition rates are relatively insensitive to pressure in the vicinity of the optimum value. Thus a good strategy for densification might be to fix the pressure somewhat above the optimum value based on the initial pore size and to hold this constant during the process. The pressure would then be a bit high early in the process, but would be a bit low toward the end. At this fixed pressure, the temperature history alone can then be varied to obtain the desired final uniformity and final degree of densification. This strategy should yield mean deposition rates comparable to those of a full optimization of the pressure history, but again avoids simultaneous variation of both pressure and temperature. Decoupling the problem in this way should greatly reduce the experimental or computational effort needed to obtain an optimum process cycle.

The recommended optimum pressures for these coating and densification strategies are in good agreement with previous numerical results. Ofori and Sotirchos [14] determined the optimum pressure and temperature to densify a preform to some specified extent in the minimum time, subject to a constraint on the deposition uniformity. That analysis considered the deposition of silicon carbide from a mixture of hydrogen and methyltrichlorosilane (MTS) under isobaric, isothermal conditions. Here we compare their results with the optimum pressure given by Eq. (47). The required molecular properties of the two gases are $m_1 = 149$ g/mol, $m_2 = 2$ g/mol, $\sigma_1 = 5.87$ Å, and $\sigma_2 = 2.83$ Å, where the subscript 1 refers to MTS and 2 refers to hydrogen [15]. By Eq. (A5) of the Appendix, these values give a diffusivity ratio of $\alpha = 11.2$ for all species mole fractions. The remaining required parameters are $N = 6.02 \times 10^{23}$ molecules/mol and $E_a = 120$ kJ/mol [14]. These values yield $p = 59$ kPA for $d = 50$ μm. For $d = 5$ μm and $d = 0.5$ μm, Eq. (47) gives $p = 590$ kPa and $p = 5.9$ MPa.

The optimum pressures read from Figs. 1, 5, 7 and 9 of the Ofori and Sotirchos paper range from about 40 to 90 kPa for $d = 50$ μm, from about 400 to 900 kPa for $d = 5$ μm, and from about 4 to 9 MPa for $d = 0.5$ μm. Although it is difficult to pick these optima very accurately from the figures, these ranges of values are in excellent agreement with the values obtained from Eq. (47). Aside from this good quantitative agreement, we note that their optimum pressures consistently exhibit the inverse dependence on pore size given by Eq. (47). Their Figs. 1, 5, 7, 8, 13 and 15 further suggest that the optimum pressure for densification, even under a uniformity constraint, does not depend on transport properties of the preform, the pre-exponential deposition rate constant, or the specified deposition uniformity. This again is in agreement with Eq. (47).

Sample Calculations

To illustrate the application of this analysis, we consider the sample problem of depositing a thin coating of boron nitride on fibers within a preform using boron trichloride and ammonia. The preform half-thickness is $a = 5$ mm, fiber diameter is $d_f = 10$ μm, and the porosity is $\epsilon = 0.6$. From simple geometry, the preform specific surface area is given by $s_v = 4(1-\epsilon)/d_f = 1.6 \times 10^{-5}$ m^{-1}. Likewise, the effective pore diameter is given by $d = 4\epsilon/s_v = 15$ μm [16]. For simplicity we assume that the fibers are arranged in a regular hexagonal array. Effective thermal conductivities, equivalent to the effective diffusivity, have been computed for this geometry. The result at a fiber porosity of 0.6 is $D' = 0.43$ [17].

Boron trichloride and ammonia react rapidly in the gas phase to form Cl_2BNH_2 and HCl [18]. For arbitrary flow rates of these two gases, this gas-phase reaction can be described by

$$BCl_3 + G\,NH_3 \rightarrow HCl + Cl_2BNH_2 + (G-1)\,NH_3 \quad (48)$$

where G is the ratio of the volumetric flow rate of ammonia to that of the boron trichloride. The Cl_2BNH_2 species is then the deposition precursor for the surface reaction given by

$$Cl_2BNH_2 \rightarrow BN(s) + 2\ HCl \qquad (49)$$

From these two reactions the reactant fraction is given by $f_a = 1/(G+1)$ provided that the reactant flow rates are sufficiently large that product gases do not significantly accumulate inside the furnace. Under this restriction, the reactant fraction is $f_a = 0.33$ for a relative flow rate of $G = 2$. From the surface reaction we see that two moles of gas-phase product are produced for each mole of reactant, giving $\psi = 1$ and a normalized reactant yield of $\psi^* = \psi f_a = 0.33$. The parameters $E - a$ and b for the surface reaction probability are approximately 147 kJ/mol and 446, respectively [19].

The diffusivity ratio, α, is computed using kinetic theory,

$$\frac{1}{\alpha} = \frac{1}{1-x_1} \sum_{j=2}^{n} x_j \left(\frac{\sigma_1 + \sigma_j}{2\sigma_1} \right)^2 \left(\frac{2m_j}{m_1 + m_j} \right)^{1/2} \qquad (50)$$

where the mole fractions of Cl_2BNH_2, NH_3 and HCl are $x_1 = x_2 = x_3 = 0.33$, and the corresponding species molecular weights are 98, 17, and 36 g/mol. The molecular diameters are 4.7, 2.6 and 3.3 Å, respectively [15]. These values yield $\alpha = 2.3$. A more accurate estimate of the diffusivity ratio could be computed using, for example, the more complete Chapman-Enskog theory for the transport properties of gases.

Using these basic parameters, the normalized preform thickness can be computed from Eq. (13) as $\xi = 1.66 \times 10^4$. The reference pressure and temperature given by Eq. (20) are $p_R = 38$ kPa (290 torr) and $T_R = 17680$ K, yielding a reference deposition rate of $S_R = 5.39 \times 10^4$ mol/m^{2}s. Now from Fig. 6, or from the solution of Eqs. (18), (29) and (30), the optimum conditions are given by $p^* = 2$ and $T^* \approx 0.0465$, corresponding to a dimensional optimum pressure of 77 kPa (580 torr) and optimum temperature of 549 C. The deposition modulus at these conditions is $\beta \approx 4.18$, the associated uniformity is $U \approx f_c/f_a = 0.216$, and the normalized centerline deposition rate is $S^{**} \approx 0.253$. This corresponds to a dimensional deposition rate of $S = S_R S^{**}/\xi^2 = 1.74 \times 10^{-5}$ mol/m^{2}s. At a BN solid density of 2.0 g/cm^3 and molecular weight of 24.8 g/mol, this gives a centerline deposition rate of 0.78 μm/hr.

Note that even the small normalized reaction yield of our sample problem significantly affects the optimum conditions and maximum deposition rate. If we take $\psi^* = 0$, but leave all other problem parameters unchanged, the resulting optimum temperature increases to 551 C and the maximum centerline deposition rate increases to 0.92 μm/hr. Thus a normalized reaction yield of only $\psi^* = 0.33$ has reduced the maximum deposition rate by over 15%.

As illustrated in Fig. 7, the deposition rate is insensitive to pressure over a wide range of values near the optimum. In our sample problem, reducing the pressure an order of magnitude to 7.7 kPa (58 torr) still gives a maximum centerline deposition rate of 0.67 μm/hr at an optimum temperature of 642 C. Again reducing the pressure to 770 Pa (5.8 torr) yields a maximum deposition rate of 0.23 μm/hr at a temperature of 704 C. Thus a pressure two orders of magnitude below the optimum value only reduces the maximum deposition rate by about a factor of three in this sample problem. However, reducing the pressure just one more decade, to 77 Pa (580 mtorr), yields a maximum centerline deposition rate of just 0.030 μm/hr at an optimum temperature of 717 C. At this pressure the deposition rate is falling about linearly with the pressure and will continue this behavior as the pressure is further reduced.

Over the pressure range from about 0.8 to 80 kPa (6 to 600 torr), the maximum centerline deposition rate increases by about a factor three while the optimum temperature decreases from 642 to 549 C. This insensitivity to pressure may permit placing additional constraints on the process conditions without seriously reducing deposition rates. For example, the morphology of deposited BN may depend on the process temperature. If higher temperatures yield the desired morphology, then lower pressures may be preferred. Likewise, the gas-phase reaction of boron trichloride and ammonia is known to precipitate solid ammonium chloride if pressures are sufficiently high. In this case, the total pressure may need to be reduced below the optimum value. By reducing the pressure and slightly increasing the temperature, precipitation can be avoided, again without significantly reducing the deposition rate.

Summary

To help optimize CVI process conditions, we have derived analytical expressions describing the pressure and temperature giving the maximum centerline deposition rate for a first-order deposition reaction involving a single reactive species. These analytical

expressions account for both diffusive and advective transport and both ordinary and Knudsen diffusion. The resulting optimum conditions are a function of only two dimensionless parameters: the normalized preform thickness; and the normalized reaction yield indicating the relative importance of advective transport away from the preform center due to the evolution of product gases from the deposition reaction. Although these results also have use in optimizing preform densification, the analysis employed here is strictly applicable only to fiber coating processes wherein the coating thickness remains small compared to the original fiber diameter.

The optimum pressure is obtained in closed form. Its value is proportional to the activation energy of the deposition reaction and inversely proportional to the characteristic preform pore size. Surprisingly, the optimum pressure does not depend on the preform thickness, specific surface area or effective diffusivity, nor does it depend on the reaction yield.

Optimum temperatures are obtained from the analytical expressions describing the optimum conditions, along with the derivative of the centerline reactant fraction with respect to the deposition modulus. Using an analytical solution to provide the derivative of the centerline reactant fraction, a closed-form implicit expression for the optimum temperature is obtained for the special case of no normalized reaction yield. For the more general case, this derivative is computed from numerical solutions to the equations governing transport and deposition. Optimum temperatures are presented graphically for a very wide range of the normalized preform thickness and normalized reaction yield.

As we would expect, the optimum temperature and maximum centerline deposition rate depend strongly on the preform thickness. Surprisingly, however, the deposition modulus and deposition uniformity at the optimum conditions are nearly independent of the thickness for a given normalized reaction yield. This provides a simple means of identifying optimum conditions for preforms of varying thickness once the optimum is known for a single case. The optimum temperature for a new thickness is obtained when the deposition uniformity is unaltered, as determined experimentally or by using a simple algebraic relation to give the same deposition modulus for the new preform thickness.

The optimum conditions yield a weak one-sided maximum of the centerline deposition rate. The deposition rate falls linearly at pressures well below the optimum value, but remains nearly constant at all values above. The reason for this behavior lies in the tradeoff between the linear pressure dependence of the deposition reaction and the nonlinear pressure dependence of the diffusivity in the transition between the ordinary and Knudsen regimes. At very low pressures, Knudsen numbers are large, Knudsen diffusion is dominant, and the centerline deposition rate at the optimum temperature increases linearly with increasing pressure. At very high pressures, however, Knudsen numbers are small, ordinary diffusion is dominant, and the maximum centerline rate falls weakly as the pressure becomes infinite.

Conditions yielding the maximum centerline deposition rate give a deposition uniformity of only about 25%. That is, the deposition rate at the preform surface is roughly four times that at its center. Since this is probably not acceptable for some coating applications, we have also examined the influence on the optimum conditions of a constraint on the deposition uniformity. Using the method of Lagrange multipliers, we find that the optimum pressure in this constrained maximization of the centerline deposition rate is the same as that obtained in the unconstrained case. This surprising result suggests that a good strategy for optimizing both fiber coating and densification processes is to fix the pressure at the optimum value, and then vary only the temperature or temperature history to obtain the desired final state of the preform. The recommended optimum pressure, obtained here analytically, is in good agreement with the values obtained in a previous numerical analysis of the optimum conditions for preform densification when the deposition uniformity is constrained.

Although the discussions presented here focus on fibrous preforms, all of these results are equally applicable to particulate materials.

Nomenclature

a	preform thickness
b	deposition reaction pre-exponential constant
d	inter-fiber pore size
D	effective binary diffusivity
D'	effective diffusivity of porous preform
D_m	effective ordinary binary diffusivity
D_{Kn}	reactant Knudsen diffusivity $(D_{\mathrm{Kn}} = \overline{v}d/3)$
E_a	deposition reaction activation energy
f	reactive species mole fraction
Kn	Knudsen number $(\mathrm{Kn} = \lambda/d)$
m	reactive species molecular weight
N	Avogadro number
p	total gas pressure
R	ideal gas constant
S	surface deposition rate

T temperature
u fluid speed
U deposition uniformity $(U = f_c/f_a = f_c^*)$
$\overline{v}$ reactant mean molecular speed
x transverse position
z normalized transverse position $(z = x/a)$
α ratio of diffusivities
β deposition modulus
λ reactant mean free path
ξ normalized preform thickness
ρ total molar density
σ reactive species molecular diameter
ϕ reaction probability
ψ net molar yield of deposition reaction

Subscripts and Superscripts
a at preform surface
c at preform center
R reference value for normalization
$*$ asterisk denotes normalized variable

Acknowledgment

The authors wish to thank Dr. G. S. Thurston for sharing with us his broad experience in composites manufacturing. This work was funded in part by the Defense Advanced Research Projects Agency (DARPA) High Temperature Structural Materials Program and in part by the US Department of Energy Office of Industrial Technologies, Advanced Industrial Materials Program.

References

1. P. McAllister and E. E. Wolf, "Modeling of Chemical Vapor Infiltration of Carbon in Porous Carbon Substrates," *Carbon*, **29**, 387 (1991).
2. B. W. Sheldon and T. M. Besmann, "Reaction and Diffusion Kinetics During the Initial Stages of Isothermal Chemical Vapor Infiltration," *J. Am. Ceram. Soc.*, **74**, 3046 (1991).
3. V. Cholet and L. Vandenbulcke, "Chemical Vapor Infiltration of Boron Nitride Interphase in Ceramic Fiber Preforms: Discussion of Some Aspects of the Fundamentals of the Isothermal Chemical Vapor Infiltration Process", *J. Am. Ceram. Soc.*, **76**, 2846 (1993).
4. G. Savage, *Carbon-Carbon Composites*, p. 372, Chapman and Hall, London, (1993).
5. R. J. Melkote and K. F. Jensen, "Gas Diffusion in Random-Fiber Substrates," *AIChE J.*, **35**, 12 (1989).
6. B. W. Sheldon and H. C. Chang, "Minimizing Densification Times During the Final Stage of Isothermal Chemical Vapor Deposition," *Cer. Trans.*, **42**, 81 (1994).
7. S. V. Sotirchos, "Dynamic Modeling of Chemical Vapor Infiltration," *AIChE J.*, **37**, 1365 (1991).
8. S. Vaidyaraman, W. J. Lackey, P. K. Agrawal and T. L. Starr, "1-D Model for Forced Flow Thermal Gradient Chemical Vapor Infiltration Process for Carbon-Carbon Composites," *Carbon*, **34**, 9, 1123 (1996).
9. C. Bonsanquet, British T. A. Report, BR 507 (1944). See also W. G. Pollard and R. D. Present, *Phys. Rev.*, **73**, 762 (1948).
10. R. B. Bird, W. E. Stewart and E. M. Lightfoot, *Transport Phenomena*, pp. 510 and 571, John Wiley & Sons, New York, NY (1960).
11. E. W. Thiele, "Relation Between Catalytic Activity and Size of Particle, *Ind. Eng. Chem.*, **31**, 7, 910 (1939).
12. S. K. Griffiths and R. H. Nilson, "Deposition Uniformity, Particle Nucleation and the Optimum Conditions for Chemical Vapor Deposition in Multiwafer Furnaces," J. Electrochem. Soc., **144**, 4, 1399 (1997).
13. W. Kaplan, *Advanced Calculus*, p. 184, Addison-Wesley, Reading, MS (1973).
14. J. Y. Ofori and S. V. Sotirchos, "Optimal Pressures and Temperature for Isobaric, Isothermal Chemical Vapor Infiltration," *AIChE J.*, **42**, 10, 2828 (1996).
15. R. C. Reid, J. M. Prausnitz and T. K. Sherwood, *The Properties of Gases and Liquids*, pp. 24 and 679, McGraw-Hill, New York, NY, (1977). MTS properties were computed based on critcal conditions of 517 K and 3.28 MPa and an estimated acentric factor of 0.26.
16. G. L. Vignoles, "Modeling Binary, Knudsen and Transition Regime Diffusion Inside Complex Porous Media," *J. Phys. Colloq. IV*, **C5**, 159 (1995).
17. W. T. Perrins, D. R. McKenzie and R. C. McPhedran, "Transport Properties of Regular Arrays of Cylinders," *Proc. Roy. Soc.*, A **369**, 207 (1979).
18. M. D. Allendorf and T. H. Osterheld, "Chemical Reactions in the CVD of Boron Nitride from BCl_3 and NH_3," *Proc. 13th Int. Conf. Chem. Vapor Dep.*, **96-5**, 16 (1996).
19. N. Patibandla and K. L. Luthra, "Chemical Vapor Deposition of Boron Nitride," *J. Electrochem. Soc.*, **139**, 12, 3558 (1996).

Appendix

The parameter α is the ratio of the effective binary coefficient of ordinary diffusion for the reactive species and the mixture of other furnace gases to the coefficient of ordinary self diffusion for the reactive species. Denoting the coefficient for the mixture as

D_{1m} and the coefficient for the reactive species only as D_{11}, this may be written

$$\alpha = \frac{D_{1m}}{D_{11}} \tag{A1}$$

The values of the terms on the right of Eq. (A1) may be computed by any number of methods, ranging from the very simple to very complete. Here we consider a very simple method based on kinetic theory and the rigid sphere approximation.

The effective binary coefficient of ordinary diffusion for the reactive species in a gas mixture may be expressed as [10]

$$\frac{1 - x_1}{D_{1m}} = \sum_{j=2}^{n} \frac{x_j}{D_{1j}} \tag{A2}$$

where x_j are the mole fractions of each species, and D_{1j} is the binary coefficient of ordinary diffusion for the reactive species paired with species j. In this case the subscript $j = 1$ refers to the species of interest, while $j = 2$ and above refer to all other species in the mixture. Combining Eqs. (A1) and (A2) yields an expression for α in terms of the binary coefficients of diffusion only.

$$\frac{1}{\alpha} = \frac{1}{1 - x_1} \sum_{j=2}^{n} x_j \frac{D_{11}}{D_{1j}} \tag{A3}$$

Now assuming the hard sphere molecular behavior, the ratio D_{11}/D_{1j} may be written as

$$\frac{D_{11}}{D_{1j}} = \left(\frac{\sigma_1 + \sigma_j}{2\sigma_1} \right)^2 \left(\frac{2m_j}{m_1 + m_j} \right)^{1/2} \tag{A4}$$

where σ_j and m_j are the atomic diameter and molecular weight of the jth mixture species. Note that neither the pressure nor temperature appear in this relation because D_{11} and D_{1j} always share the same functional dependence on both. Finally, combining Eqs. (A3) and (A4) gives the desired expression for α.

$$\frac{1}{\alpha} = \frac{1}{1 - x_1} \sum_{j=2}^{n} x_j \left(\frac{\sigma_1 + \sigma_j}{2\sigma_1} \right)^2 \left(\frac{2m_j}{m_1 + m_j} \right)^{1/2} \tag{A5}$$

We now see that the rigid sphere molecular model gives a value for α that depends only on the mixture composition and the molecular diameter and weight of all the mixture species. However, a more rigorous treatment based on Chapman-Enskog theory would yield a slight pressure and temperature dependence for the ratio D_{11}/D_{1j}. The value of α in that case would also show a weak dependence on the process conditions for a fixed mixture composition.

We need also keep in mind that the process conditions may directly influence the composition of the furnace gas mixture, so in this sense the diffusivity ratio α will vary with pressure and temperature due to variations in x_j, whether or not the ratios D_{11}/D_{1j} are constant. In this case, the present analysis may be combined with a simple zero or one-dimensional auxiliary model of reactant injection and transport within the furnace. Using the specified injection rate and assumed trial values for the optimum pressure and temperature, the results presented here can be used with such an auxiliary model to compute the composition of the furnace gas mixture. From this estimate of the composition, a value for α and new candidate values for the optimum pressure and temperature can then be calculated. This computational procedure may then be repeated, each time using the final estimates of the optimum conditions as initial guesses for the next iteration. This method should converge quickly because the value of α is a fairly weak function of the composition.

UNLIMITED RELEASE
INITIAL DISTRIBUTION

K. F. Jensen
Massachusetts Institute of Technology
Building 6-469
Chemical Engineering
Cambridge, MA 02139

Sunil Shah
RelMan, Inc.
3255-2 Scott Blvd., Suite 103
Santa Clara, CA 95054

W. Foslien
Honeywell Technology Center
3660 Technology Drive
Minneapolis, MN 55418

C. Sorrell
Office of Advanced Industrial Concepts, EE-232
U.S. Dept. of Energy
1000 Independence Avenue
Washington, D.C. 20585

B. W. Sheldon
Division of Engineering, Box D
182 Hope Street
Providence, RI 02912

T. M. Besmann
Oak Ridge National Laboratory
P.O. Box 2008
Oak Ridge, TN 37831-6060

M. Zachariah
National Institue of Standards and Technology
Building 221, Room B312
Gaithersburg, MD 20899

G. S. Thurston
Integrated Systems, Inc.
300 W. Main Street
Northborough, MA 01532

S. V. Sotirchos
Department of Chemical Engineering
University of Rochester
Rochester, NY 14627

C. B. Shumaker
DuPont Lanxide Composites, Inc.
1300 Marrows Road
P.O. Box 6077
Newark, DE 19714-6077

R. J. Kee
Engineering Division
Colorado School of Mines
Golden, CO 80401-1887

Textron Specialty Materials
2 Industrial Avenue
Lowell, MA 01851
Attn: J. E. Niemoller
R. Suplinskas

0513 R. J. Eagan, 1000
Attn: P. L. Mattern, 1100
J. Q. Searcy, 1400
H. J. Saxton, 1800
9001 T. O. Hunter, 8000
Attn: M. E. John, 8100
A. West, 8200
R. C. Wayne, 8400
T. M. Dyer, 8700
D. L. Crawford, 8900
9403 J. M. Hruby, 8230
9054 W. J. McLean, 8300
Attn: W. Bauer, 8302
L. A. Rahn, 8351
F. P. Tully, 8353
G. A. Fisk, 8355
R. W. Carling, 8362
9042 G. H. Evans, 8345
9042 J. F. Grcar, 8345
9042 S. K. Griffiths, 8345 (10)
9042 C. M. Hartwig, 8345
9042 W. G. Houf, 8345
9042 R. S. Larson, 8345
9042 E. Meeks, 8345
9042 C. D. Moen, 8345
9042 R. H. Nilson, 8345 (10)
9042 P. A. Spence, 8345
9052 M. D. Allendorf, 8361 (5)
9052 D. R. Hardesty, 8361
9053 S. R. Vosen, 8362
0834 A. C. Ratzel, 9112
0834 W. L. Hermina, 9111
0834 M. R. Baer, 9112
9021 Technical Communications, 8535
for OSTI (10)
9021 Technical Communications, 8535
8099 Technical Library, 13414 (4)
9018 Central Technical Files, 8523-2 (3)